Assimilating remote sensing observations of leaf area index and soil moisture for wheat yield estimates: An observing system simulation experiment

G. S. Nearing,[1] W. T. Crow,[2] K. R. Thorp,[3] M. S. Moran,[4] R. H. Reichle,[5] and H. V. Gupta[1]

Received 18 September 2011; revised 23 January 2012; accepted 26 March 2012; published 17 May 2012.

[1] Observing system simulation experiments were used to investigate ensemble Bayesian state-updating data assimilation of observations of leaf area index (LAI) and soil moisture (θ) for the purpose of improving single-season wheat yield estimates with the Decision Support System for Agrotechnology Transfer (DSSAT) CropSim-Ceres model. Assimilation was conducted in an energy-limited environment and a water-limited environment. Modeling uncertainty was prescribed to weather inputs, soil parameters and initial conditions, and cultivar parameters and through perturbations to model state transition equations. The ensemble Kalman filter and the sequential importance resampling filter were tested for the ability to attenuate effects of these types of uncertainty on yield estimates. LAI and θ observations were synthesized according to characteristics of existing remote sensing data, and effects of observation error were tested. Results indicate that the potential for assimilation to improve end-of-season yield estimates is low. Limitations are due to a lack of root zone soil moisture information, error in LAI observations, and a lack of correlation between leaf and grain growth.

Citation: Nearing, G. S., W. T. Crow, K. R. Thorp, M. S. Moran, R. H. Reichle, and H. V. Gupta (2012), Assimilating remote sensing observations of leaf area index and soil moisture for wheat yield estimates: An observing system simulation experiment, *Water Resour. Res.*, *48*, W05525, doi:10.1029/2011WR011420.

1. Introduction

[2] Dynamic crop models, such as the Decision Support System for Agrotechnology Transfer crop simulation model (DSSAT) [*Hoogenboom et al.*, 2004], are used to aid decision making under uncertainty [*Jones et al.*, 2003]. For instance, DSSAT is used by the insurance industry to predict regional crop yields on a seasonal basis. Crop simulation models have an advantage over empirical models of agricultural productivity in that they can react dynamically to changes in local conditions in a physically and biologically meaningful way. However, because of uncertainties in model representations of real-world systems and because of uncertainties inherent in input data regarding soils, cultivar genetics and weather, any model-based estimate of agricultural yield will be subject to error. One approach to mitigating this type of error is to constrain model simulations using remote sensing observations through a process of data assimilation [*Liu and Gupta*, 2007].

[3] Remote sensing measurements related to agriculture generally contain information about weather, vegetation or soil. Information about weather is used to force crop simulations directly. Remotely sensed information about vegetation often comes in the form of a leaf area index (LAI ($m^2\ m^{-2}$) [e.g., *Knyazikhin et al.*, 1999]), which is a crop model component related to canopy cover. Similarly, soil moisture is a model state variable that acts as the primary control on plant water stress and observations of volumetric moisture content (θ ($m^3\ m^{-3}$)) in the top few centimetres of soil (θ_1) are available from remote sensing sources (AMSR-E [*Njoku et al.*, 2003], SMOS [*Kerr et al.*, 2010], and SMAP [*Entekhabi et al.*, 2010]). Together LAI and SW observations provide complementary information for agricultural monitoring.

[4] There are many types of data assimilation which are common in agronomy [*Moulin et al.*, 1998; *Prévot et al.*, 2003]. This work investigates the potential for ensemble Bayesian state-updating filters [*McLaughlin*, 2002] to mitigate modeling uncertainty on end-of-season wheat yield estimates. Conceptually, ensemble Bayesian filters operate on the principle that a probability density function (pdf) representing uncertainty in model states can be approximated by a discrete set of model simulations, and that a pdf of model predictions can be estimated using Monte Carlo integration to marginalize uncertainty in model states. From a Bayesian perspective, the physical model provides

[1]Department of Hydrology and Water Resources, University of Arizona, Tucson, Arizona, USA.
[2]Hydrology and Remote Sensing Laboratory, ARS, USDA, West Beltsville, Maryland, USA.
[3]Arid-Land Agricultural Research Center, ARS, USDA, Maricopa, Arizona, USA.
[4]Southwest Watershed Research Center, ARS, USDA, Tucson, Arizona, USA.
[5]NASA Goddard Space Flight Center, Greenbelt, Maryland, USA.

0043-1397/12/2011WR011420

context (a prior and likelihood) for interpreting information contained in remotely sensed data.

[5] Currently, a robust understanding of the response of physically based model estimates of agricultural yield to state-updating assimilation remains lacking. The first step in this process is to perform a controlled synthetic data study, also called an observing system simulation experiment (OSSE) [*Arnold and Dey*, 1986], which will allow for an analysis of interactions between uncertainty, observations and the model. Although both *Pauwels et al.* [2007] and *Pellenq and Boulet* [2004] present OSSEs which investigate the assimilation of LAI and/or θ_1 into crop simulation models, these studies assess the effects of assimilation on model states; neither investigates the impact of data assimilation on yield estimates. *de Wit and van Diepen* [2007] present a case study on the effects of assimilating θ_1 observations on yield estimates; however, this does not provide sufficient statistical and methodological control to differentiate limitations imposed by the model, the assimilation algorithm, and uncertainty in model inputs and observations.

[6] We present a set of OSSEs which assess LAI and θ assimilation for improving DSSAT CropSim-Ceres wheat yield estimates in a controlled synthetic environment. This allows for an understanding of model response to state updating and a delineation of the effects of modeling uncertainty, filter error, and observation error. This investigation provides a benchmark for interpreting the results of case studies [e.g., *de Wit and van Diepen*, 2007] and a foundation on which to direct the development of agricultural models and remote sensing algorithms aimed at predicting yield.

2. Methods

[7] Several experiments are presented. First, modeling uncertainty was partitioned into isolated sources: weather inputs, soil parameters and initial conditions, cultivar parameters, and model state equations. Synthesized remote sensing observations were assimilated using the ensemble Kalman filter (EnKF) [*Evensen*, 2003] and the sequential importance resampling filter (SIRF) [*Gordon et al.*, 1993], and mean yield predictions from these filters were assessed. In addition, observations with variable error characteristics were assimilated to test the effects of observation error on EnKF and SIRF results. Sections 2.1–2.4 describe the model, data assimilation filters, and sets of numerical experiments.

2.1. The DSSAT CropSim Ceres Wheat Model

[8] DSSAT is a collection of independent crop growth modules supported by a land process wrapper. Integration takes place on a daily time step and the forcing data required are daily maximum and minimum temperature, daily integrated solar radiation and daily cumulative precipitation.

[9] DSSAT soil layering is user defined; we used nine layers with one surface layer representing the 0–5 cm of soil typically assumed to be visible to L band wavelength satellites and a set of lower layers reaching a total depth of 1.8 m. DSSAT soil moisture is calculated using a Richie-type soil water balance [*Richie*, 1998], which employs a curve number approach to partitioning runoff and updates the water content of each soil layer on the basis of a set of linear drainage equations. The soil surface parameters are: a runoff curve number, an upper limit on evaporation, a drainage rate parameter, and albedo. Soil layers are parametrized by saturated water content (porosity), drained upper limit (field capacity), lower limit, saturated hydraulic conductivity, and a root growth factor. Similar to *Mo et al.* [2005], we used the soil water balance routines but did not simulate the soil nitrogen balance or any management decisions. This was done because it is impossible to presume that information about these aspects of agricultural development would be available at remote sensing scales.

[10] The CropSim-Ceres module (CC) simulates wheat crops. The CC models yield as a function of a grain weight state. Grain growth is developmentally dependent on daily development units, which are a function of mean daily temperature and daily cumulative solar radiation, a temperature control factor, vegetation biomass (β (kg/plant)) defined as the sum of mass storage model states stem weight, leaf weight, and reserves weight, and model parameters. The most important crop model parameters are related to the cultivar: vernalizing duration, which specifies the number of days of optimum temperature necessary for vernalization; photoperiod response, which specifies the percent reduction in photosynthesis for every 10 h reduction in photoperiod; grain filling phase duration in growing degree-days (°C days); number of kernels per unit plant weight (number g^{-1}); the standard kernel size (mg); the standard tiller weight (g); and the photoperiod interval between leaf tip appearances.

[11] In contrast to grain weight, LAI is a function of the model state plant leaf area which is developmentally dependent on a temperature control factor and has a potential value set by the number of plant leaves, which is in turn determined at each time step by the cumulative sum of daily development units. Again, in contrast to grain growth, potential daily leaf growth is attenuated by an additive factor proportional to water stress, $S_w \in [0, 1]$, so that a stress factor of 0 indicates potential growth and a stress factor of 1 indicates no growth. Potential grain growth is not modified in this way; the other components of biomass are affected indirectly by stress through leaf assimilation of plant carbon reserves. Water stress is the ratio of total root water uptake to potential transpiration, which is a fraction of potential evapotranspiration calculated according to the Priestley-Taylor method [*Priestley and Taylor*, 1972]. Root water uptake from each layer is a function of the difference between soil moisture state and the lower limit parameter. Thus when sufficient soil moisture is available to supply transpiration demand, water stress is zero. Given the way model develops vegetation and grain components of the wheat plant, we know that LAI and θ will inform yield by informing β.

[12] The model state vector contains all of the internal dynamic model variables necessary to transition the simulation from one time step to the next, that is, all of the Markov information. More specifically, at given time t, state ($\mathbf{x}_t$) is a function of the state at the previous time ($\mathbf{x}_{t-1}$), forcing data at the current time ($\mathbf{u}_t$), and time-invariant model parameters (ϑ) according to the state transition relationship $\mathcal{M}_x(\cdot)$:

$$\mathbf{x_t} = \mathcal{M}_x(\mathbf{x}_{t-1}, \mathbf{u}_t, \vartheta). \tag{1a}$$

The combined land process wrapper and CC Markov state vector has 97 components (Tables 1 and 2). The model output vector at time t ($\mathbf{y}_t$; here we use the term output to refer to model predictions which correspond directly with observations) is calculated according to the relationship $\mathcal{M}_y(\cdot)$ as a function of the current state, current inputs and parameters:

$$\mathbf{y_t} = \mathcal{M}_y(\mathbf{x}_t, \mathbf{u}_t, \vartheta). \quad (1b)$$

For our purposes, the output vector contained the quantities $\theta_{1:9}$ (soil moisture in each of 9 soil layers) and LAI; $\theta_{1:9}$ are also state variables so $\mathcal{M}_y(\cdot)$ simply preserves these values through identity relationships. LAI is not a state variable because its value is calculated independently at each time step as a function of the state plant leaf area.

2.2. The Ensemble Kalman Filter

[13] The EnKF is commonly used for state updating in moderately nonlinear geophysical models [*Reichle*, 2008]. It estimates the model state pdf by drawing N_{ens} samples from a joint uncertainty pdf over model parameters, forcing data, and state perturbations, and then propagates this sample through time using the model equations. This set of model simulations is the *ensemble*. At every observation time, the EnKF updates the state pdf on the basis of the assumptions that all model states are linearly related to model output and that uncertainty in model states, model output, and observations can be quantified by second-order pdf approximations. Because the method has been widely discussed, we only present a brief overview and follow a variation on the formulation of *Houtekamer and Mitchell* [2001].

Table 1. The Decision Support System for Agrotechnology Transfer (DSSAT) Markov State Vector (33 Components)

Component	Description	Units
ATOT	Sum of last 5 days soil temperature	C
CANHT	Canopy height	m
DRN	Drained soil water	cm
EO	Potential evaporation	mm d^{-1}
EOP	Potential plant transpiration	mm d^{-1}
EORATIO	Increase in evaporation per unit LAI	mm d^{-1}
EOS	Potential soil evaporation	mm d^{-1}
EP	Plant transpiration	mm d^{-1}
ES	Soil evaporation rate	mm d^{-1}
FRACRTS	Fraction of soil contact w/roots	
KSEVAP	Light extinction coefficient (evaporation)	
KTRANS	Light extinction coefficient (transpiration)	
PORMIN	Minimum pore space for O_2 to plants	m^3 m^{-3}
RLV	Root volume by soil layer	m^3 m^{-3}
RWUMX	Maximum uptake per unit root length	m^3 m^{-3}
SNOW	Snow accumulation	mm
SRFTEMP	Surface soil temperature	°C
SSOMC	Soil Carbon	kg ha^{-1}
ST	Soil temperature	°C
STGDOY	Stage transition dates	day
SUMES1	Cumulative stage 1 soil evaporation	mm
SUMES2	Cumulative stage 2 soil evaporation	mm
SW	Soil water	m^3 m^{-3}
SWDELTS	Drainage rate	m^3 m^{-3}
SWDELTU	Change in SW due to evaporation	m^3 m^{-3}
SWDELTX	Change in SW due to plant uptake	m^3 m^{-3}
TMA	Last 5 days of soil temperature	°C
TRWU	Total root water uptake	mm
TRWUP	Total potential root water uptake	m^3 m^{-3}
TSOILEV	Duration stage 2 evaporation	days
TSS	Number of days with saturated soil	days
UPFLOW	Upward flow due to evaporation	cm
WINF	Infiltration	mm

Table 2. The CropSim-Ceres Wheat Module Markov State Vector (64 Components)

Component	Description	Units
ADATEND	Anthesis end date	
AFLFSUM	Carbohydrate leaf factor	
CARBOC	Cumulative carbohydrate assimilated	g/plant
CHRSWT	Chaff reserves	g/plant
CHWT	Chaff weight	g/plant
CUMDU	Cumulative development units	°C days
CUMGEU	Cumulative germination units	°C days
CUMVD	Cumulative vernalization days	days
DAE	Days after emergence	
DEADWT	Dead leaf weight retained on plant	g/plant
G2	Coefficient of grain growth (modified)	mg/d °C
GEDSUM	Germination plus emergence duration	days
GESTAGE	Germination, emergence stage	
GETSUM	Germination plus emergence temperature sum	°C
GPLA	Green leaf area	cm^2/plant
GPLASENS	Green leaf area during senescence	cm^2/plant
GRNUM	Grains per plant	number/plant
GRWT	Grain weight	g/plant
ISTAGE	Current developmental stage	
ISTAGEP	Previous developmental stage	
LAGSTAGE	Lag phase for grain filling stage	
LAP	Leaf area by leaf number	cm^2/plant
LAPOT	Leaf area potentials by leaf number	cm^2/leaf
LAPS	Leaf area senesced by leaf number	cm^2/plant
LFWT	Leaf weight	g/plant
LLRSWAD	Leaf lamina reserves weight	kg ha^{-1}
LLRSWT	Leaf lamina reserves	g/plant
LLWAD	Leaf lamina weight	kg ha^{-1}
LNUMSD	Leaf number per Haun stage	
LNUMSG	Growing leaf number	
LSHAI	Leaf sheath area index	m^2 m^{-2}
LSHRSWAD	Leaf sheath reserves weight	kg ha^{-1}
LSHRSWT	Leaf sheath reserves	g/plant
LSHWAD	Leaf sheath weight	kg ha^{-1}
PARI	PAR interception fraction	
PLA	Plant leaf area	cm^2
PLTPOP	Plant Population	plants/m^2
RSTAGE	Reproductive development stage	
RSWT	Reserves weight	g/plant
RTDEP	Root depth	cm
RTWT	Root weight	g/plant
RTWTL	Root weight by layer	g/plant
SEEDRS	Seed reserves	g/plant
SEEDRSAV	Seed reserves available	g/plant
SENCL	Senesced Carbon by layer	g/plant
SENCS	Senesced Carbon added to soil	g/plant
SENLA	Cumulative senesced leaf area	cm^2/plant
SRADSUM	Cumulative radiation	MJ m^{-2}
SSTAGE	Secondary stage of development	
STRSWT	Stem reserves	g/plant
STWT	Stem weight	g/plant
TNUM	Tiller number	number/plant
TSDAT	Terminal spikelet date	
TSS	Duration of saturation	days
TTD	Thermal time over last 20 days	°C
TTNUM	Thermal time means in sum	°C days
VF	Vernalization factor	
WFG	Water stress factor for growth	
WFGC	Cumulative growth water factor	
WFLFNUM	Water stress factor for each leaf	
WFLFSUM	Cumulative water stress factor per leaf	
XSTAGE	Stage of development	
ZSTAGE	Zadok stage of development	
ZSTAGEP	Precious Zadok stage	

[14] The ensemble of model state predictions at time t is stored in $\mathbf{X_t} = [x_{t,1}, x_{t,2}, \ldots, x_{t,N_{ens}}]$, which has size $D_{stt} \times N_{ens}$ where D_{stt} is the dimension of x_t. Similarly, the ensemble of model outputs is $\mathbf{Y_t} = [y_{t,1}, y_{t,2}, \ldots, y_{t,N_{ens}}]$, which has dimensions $D_{obs} \times N_{ens}$ where D_{obs} is the dimension of the observation vector, $\mathbf{z_t}$. The observation error covariance, R_t, is required a priori and an observation sample $\mathbf{Z_t} = [\zeta_{t,1}, \zeta_{t,2}, \ldots, \zeta_{t,N_{ens}}]$ is generated according to

$$\zeta_{\mathbf{t,i}} \sim \mathrm{N}[\mathbf{z_t}, \mathbf{R_t}]. \tag{2}$$

The ensemble of EnKF updated model states, $\widehat{\mathbf{X_t}}$, is calculated as a least squares estimate based on model predictions and observations resulting in

$$\widehat{\mathbf{X_t}} = \mathbf{X_t} + \mathbf{P_t}(\mathbf{Q_t} + \mathbf{R_t})^{-1}(\mathbf{Z_t} - \mathbf{Y_t}) \tag{3a}$$

where

$$\mathbf{P_t} = \frac{(\mathbf{X_t} - \mathrm{E}[\mathbf{X_t}])(\mathbf{Y_t} - \mathrm{E}[\mathbf{Y_t}])^T}{(N_{ens} - 1)} \tag{3b}$$

is the cross covariance between ensemble deviations from mean model state and deviations from mean output and

$$\mathbf{Q_t} = \frac{(\mathbf{Y_t} - \mathrm{E}[\mathbf{Y_t}])(\mathbf{Y_t} - \mathrm{E}[\mathbf{Y_t}])^T}{(N_{ens} - 1)} \tag{3c}$$

is the covariance matrix of ensemble deviations from mean model output. Both $\mathbf{P_t}$ and $\mathbf{Q_t}$ are sampled directly from the ensemble.

[15] The finite nature of ensemble representations of uncertainty can lead to spurious updates when $\mathbf{X_t}$ contains components that are not approximately or locally linearly related to components of $\mathbf{Y_t}$. An analysis of DSSAT state and observation correlations resulted in a list of important Markov state components which have local approximately linear relationships with one or more output (Table 3, except stage timing states). This list includes all CC plant mass storage components, plant leaf area, and root volume (root accumulation is stored as a volumetric fraction rather than as a mass) as well as canopy height. Our EnKF employed a threshold filter which discarded any relationship between model states and modeled observation components with a Pearson product-moment correlation coefficient $|\rho| < 0.3$. This reduced the possibility of picking up spurious correlations.

Table 3. The State Vector Updated by the EnKF and the State Vector Perturbed by Equation (5a) to Simulate Model Structural Error[a]

State Component	Units	Dimensions
CSM states		
Soil water	$m^3\ m^{-3}$	9
Canopy height	m	1
CC states		
Root volume fraction	$cm^2\ cm^{-3}$	9
Chaff weight	g/plant	1
Stem weight	g/plant	1
Leaf weight	g/plant	1
Reserves weight	g/plant	1
Grain weight	g/plant	1
Plant leaf area	cm^2	1
Seed reserves	g/plant	1
Stage timing states		
Cumulative development units	°C days	1
Cumulative germination units	°C days	1

[a]Cumulative development units and cumulative germination units are not updated by the ensemble Kalman filter (EnKF), and grain weight is not perturbed by equation (5a).

[16] It is important to note that the CC is a set of step functions which calculate crop attributes in fundamentally different ways depending on the current stage of development. Because of these and other nonlinearities, the EnKF will not guarantee mutually consistent model states after each update since it uses a single correlation relationship to update every ensemble member regardless of the current growth stage of each particular simulation.

2.3. The Sequential Importance Resampling Filter

[17] The SIRF provides an approximate Bayesian estimate of model state uncertainty at each time step conditional on past observations without assumptions of linearity and second-order statistics. At each observation time, each ensemble member's state vector is assigned an importance weight, W_t^n, which is proportional to the posterior likelihood of that state vector conditional on all past observations:

$$W_t^n \propto \mathrm{P}(\mathbf{x_t^n}|\mathbf{z_{1:t}}) = \frac{\mathrm{P}(\mathbf{z_t}|\mathbf{x_t^n}, \mathbf{z_{1:t-1}})\mathrm{P}(\mathbf{x_t^n}|\mathbf{z_{1:t-1}})}{\mathrm{P}(\mathbf{z_t})}; \tag{4a}$$

superscripts index the ensemble member. The observations are assumed to be independent conditional on the model output, and model output is a deterministic function of model state according to (1b) so that the likelihood function relates observations to model state vectors according to

$$\mathrm{P}(\mathbf{z_t}|\mathbf{x_t^n}, \mathbf{z_{1:t-1}}) = \mathrm{P}(\mathbf{z_t}|\mathbf{y_t^n}). \tag{4b}$$

$\mathrm{P}(\mathbf{z_t}|\mathbf{y_t^n})$ is emulated by the observation uncertainty pdf, in this case Gaussian with mean $\mathbf{y_t^n}$ and covariance $\mathbf{R_t}$. The state prior, $\mathrm{P}(\mathbf{x_t^n}|\mathbf{z_{1:t-1}})$, is estimated discretely by $\mathbf{X_t}$ by the ensemble in the same way as the EnKF; this is achieved for time step t + 1 by resampling the ensemble at time step t with replacement and with probabilities proportional to $\{W_t^n\}$ resulting in an iid discrete representation of the posterior, $\mathrm{P}(\mathbf{x_t^n}|\mathbf{z_{1:t}})$. $\mathbf{X_{t+1}}$, as calculated from $\mathbf{X_t}$ by equation (1a), thus contains an iid discrete representation of the prior at time step t + 1, $\mathrm{P}(\mathbf{x_{t+1}^n}|\mathbf{z_{1:t}})$. Proportional probability weights are simply calculated as

$$W_t^n = \mathrm{P}(\mathbf{z_t}|\mathbf{y_t^n}) = \exp\left(-\frac{1}{2}(\mathbf{z_t} - \mathbf{y_t^n})^{\mathrm{T}}\mathbf{R_t^{-1}}(\mathbf{z_t} - \mathbf{y_t^n})\right). \tag{4c}$$

In our case, the simulation ensemble was updated by replacing all 97 components of each member's state vector (Tables 1 and 2) with a state vector from a different simulation (sampling with replacement). Each model retained its own parameters and forcing data.

2.4. Observing System Simulation Experiments

[18] OSSEs, as diagrammed in Figure 1, were used to assess LAI and θ assimilation potential. A group of $N_{ens} + 1$ simulations (ensemble size is discussed in section 2.4.3) was

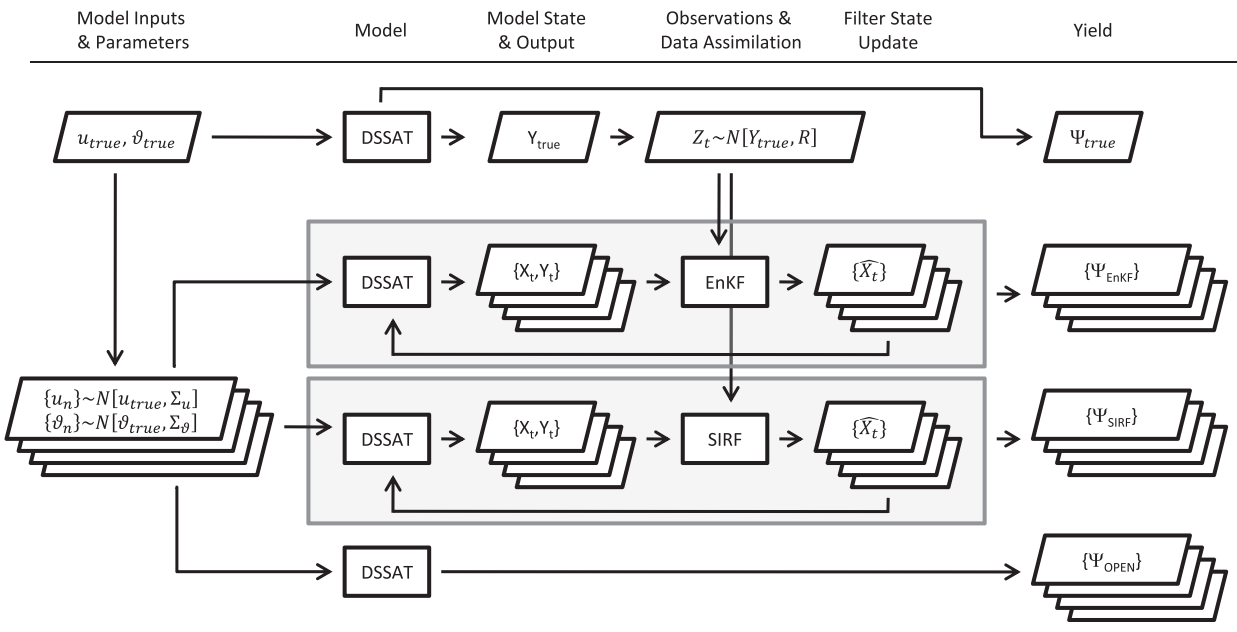

Figure 1. Observing system simulation experiment process diagram: Transparent gray boxes represent sequential importance resampling filter (SIRF) and ensemble Kalman filter (EnKF) assimilation algorithms, **u** are forcing data, ϑ are model parameters, **X** are model states, $\widehat{\mathbf{X}}$ are filter-updated model states, **Y** are modeled leaf area index (LAI) and θ, **Z** are observed LAI and θ, and Ψ is yield. **R**, Σ_ϑ, and $\Sigma_{\mathbf{u}}$ are uncertainty variances listed in Tables 4 and 5 and equation (5a).

sampled from a modeling uncertainty pdf. One of these simulations was chosen randomly as the truth system (upper path in Figure 1) leaving an N_{ens}-member prediction ensemble which was used to estimate yield with and without data assimilation. Synthetic observations were generated by sampling from an observation uncertainty distribution around the truth system output and assimilated by the EnKF and SIRF (middle paths in Figure 1). The ensemble of model simulations without data assimilation was called the open loop (bottom path in Figure 1). The open loop, EnKF and SIRF all used the same truth system and ensemble members (parameters, initial conditions and weather forcing data) and the EnKF and SIRF used the same synthetic observations.

[19] This type of OSSE was used to (1) choose an appropriate ensemble size, (2) test the effects of EnKF and SIRF assimilation on segregated and combined modeling uncertainty sources, (3) test the effects of observation uncertainty on EnKF and SIRF assimilation. Experiments 2 and 3 used the ensemble size chosen by experiment 1. In all cases except for when determining ensemble size, each OSSE was repeated fifty times by drawing separate truth systems and ensembles; this Monte Carlo repetition provided a statistically independent experiment sample. Sections 2.4.l–2.4.5 describe the modeling uncertainty pdf, the procedure for generating synthetic observations from truth system output, and these sets of experiments.

2.4.1. Modeling Uncertainty Distributions

[20] Assimilation was tested on two rain-fed wheat crops with different levels of water stress. Mean parameter and weather inputs came from field experiment data which are packaged with the DSSAT version 4.5 release: a 1975 study of a summer wheat crop conducted in Swift Current, Saskatchewan, Canada, reported by *Campbell et al.* [1977a, 1997b] and a 1974–1975 study on winter wheat conducted in Rothamsted, UK. Figure 2 plots LAI, grain weight, and water stress for both crops simulated using mean parameters outlined in Table 4 and unperturbed weather forcing data.

[21] The Swift Current summer wheat crop represents a water-limited system and yielded 104 kg ha^{-1} using mean parameters listed in Table 4; the potential, nonstressed yield was 4266 kg ha^{-1}. The mean parameter and forcing system received 153.6 mm of rainfall over a total of 95 days from planting on 25 May 1975 to maturity on 28 August 1975 and had a total evapotranspiration of 151.9 mm. The water stress factor reached a high of $S_w = 0.97$ during the ear growth stage which occurred between day 51 and day 61 after planting. Although this crop produced very little yield using the mean parameter and input values, it was often the case that simulations sampled from the parameter and input uncertainty distribution caused a substantial increase in yield.

[22] The Rothamsted winter wheat crop represents an energy-limited system and reached potential yield of 6651 kg ha^{-1} using mean parameters listed in Table 4. The system received 512.9 mm of rainfall over a total of 269 days from planting on 6 November 1974 to maturity on 6 August 1975 and had a total evapotranspiration of 381.2 mm. The water stress factor reached a high of $S_w = 0.84$ during the grain filling stage which occurred between day 240 and harvest; the water stress factor was close to 0 during all other development stages. Although this crop produced potential yield using the mean parameter and input values, it was often the case that simulations sampled from the

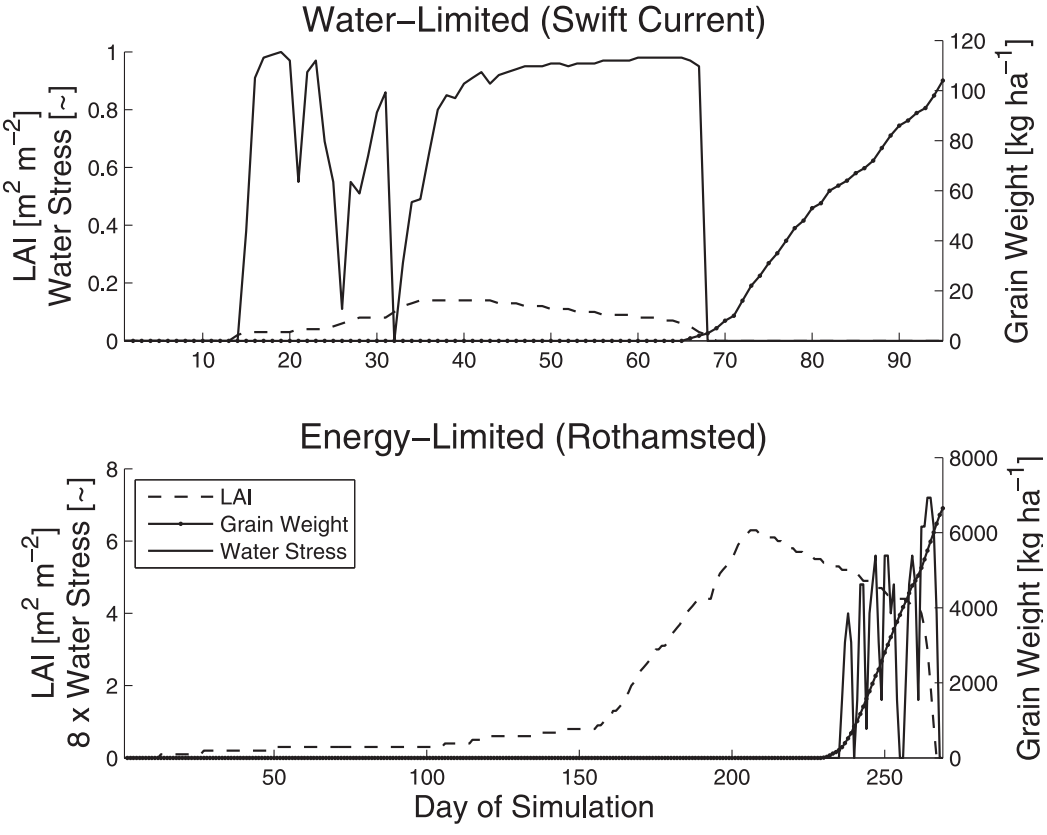

Figure 2. Baseline simulations of water-limited (Swift Current) summer wheat and energy-limited (Rothamsted) winter wheat with parameters listed in Table 4. In the Rothamsted plot, water stress is magnified by a factor of 8.

parameter and input uncertainty distribution caused a substantial decrease in yield.

[23] Weather forcing data uncertainty was emulated by perturbing daily measured weather data with values sampled form the temporally and cross-correlated joint pdf outlined in Table 5. Perturbations on solar radiation and precipitation were multiplicative lognormally distributed with a mean of 1 and standard deviations of 0.3 and 0.5, respectively; perturbations on temperature were additive Gaussian with a mean of 0 and unit variance, and the same daily perturbation was applied to daily maximum and minimum temperature. Weather perturbations were cross correlated and AR(1) (first-order autoregressive) temporally autocorrelated with correlation coefficients 1/e following *Reichle et al.* [2007, 2010]; since integration was on a daily time step, these autoregression coefficients are relevant to a daily time series.

[24] Parameter uncertainty distributions were Gaussian (approximately, due to bounds) with means, variances, and bounds listed in Table 4. Cultivar parameters are model specific; parameter files included with DSSAT release version 4.5 provided the limits and variances listed in Table 4. Variances and bounds for surface soil parameters were also estimated using a library of soil parametrizations included with DSSAT version 4.5. We used lumped parameters for the bottom eight soil layers because of a presumed lack of knowledge about subsurface soil properties. The root growth factor was assumed to decrease exponentially with depth and was parametrized by a maximum value at the surface. Porosity, saturated conductivity and residual saturation were calculated from clay and silt percentages using pedotransfer functions from *Cosby et al.* [1984]. Bulk density was calculated as a function of porosity assuming mineral density of 2.65 g cm^{-3} and drained upper limit was taken as the average of saturated and residual moisture contents. Global soils maps that provide clay and silt contents are not usually associated with useful error estimates because much of the error in soil mapping is due to sparse measurements of heterogeneous areas. Here we sampled sand and clay percentage parameters independently, each with a standard deviation of 10%; sand and clay percentages were constrained to be positive and the sum was constrained to be less than one by, when necessary, reducing both parameters by an equal amount. Given the mean sand and clay parameters from Table 4, this resulted in 95% confidence bounds which spanned approximately 18% of the soil textural triangle at and Swift Current and 25% of the soil textural triangle at Rothamsted.

[25] Model structural uncertainty was simulated by adding noise to the model state transition equations:

$$\mathbf{x}_t = \mathcal{M}_x(\mathbf{x}_{t-1}, \mathbf{u}_t, \vartheta) + \epsilon_{\mathbf{t}}; \epsilon_{\mathbf{t}} \sim \mathrm{N}[0, \Sigma_{\mathbf{x}}] \quad (5a)$$

Table 4. The (Approximately) Gaussian Probability Density Function of Uncertainty in Model Parameters and Initial Conditions

	Uncertainty					
	Mean Parameters Values					
Uncertainty Source	Swift Current	Rothamsted	Standard Deviation	Lower Bound	Upper Bound	Units
			Cultivar Parameters			
Vernalizing duration	0	60	3	0	60	days
Photoperiod response	60	67	10	0	200	%
Grain filling duration	335	515	33.5	100	1000	°C days
Kernel number	25	14	2.5	10	50	number/g
Standard kernel size	26	44	2.6	10	80	mg
Standard tiller weight	1.5	4.0	0.3	0.5	8	g
Interval between leaves	86	100	10	30	150	°C days
			Soil Parameters			
Albedo	0.10	0.14	0.05	0	1	
Upper limit evaporation	9.4	6.0	2.0	1	12	cm d^{-1}
Drainage rate parameter	0.20	0.50	0.3	0.01	0.99	1/d
Runoff curve number	84.0	60.0	10	1	99	
Root growth factor						
Layer 1 (0–5cm)	1.00	1.00	0.05	0	1	
Layers 2–9 (5–180 cm)	0.74	0.90	0.1	0	1	
Percent clay						
Layer 1 (0–5cm)	10.7	23.4	10	0	100	%
Layer 2-9 (5–180 cm)	9.2	23.4	10	0	100	%
Percent silt						
Layer 1 (0–5cm)	29.9	30.0	10	0	100	%
Layers 2–9 (5–180 cm)	29.7	30.0	10	0	100	%
Initial soil moisture						
Layer 1 (0–5 cm)	0.23	0.33	0.04	Lower limit	Saturation	$m^3\ m^{-3}$
Layers 2–9 (5–180 cm)	0.20	0.33	0.08	Lower limit	Saturation	$m^3\ m^{-3}$

This type of model error was added to those states listed in Table 3 except for grain weight, and in some cases, where specified, to the development unit stage timing states cumulative development units and cumulative germination units. It was found that perturbing the grain weight state caused irreconcilable yield error by weakening statistical relationships between observations and yield. Random state perturbations were drawn from zero-mean Gaussian distributions with heteroscedastic variances

$$\Sigma_{\mathbf{x}} = \mathrm{I}_{\mathrm{D_{stt}}} 0.02(\mathbf{x_{t-1}}), \tag{5b}$$

where $\mathrm{I}_{\mathrm{D_{stt}}}$ is the D_{stt} dimension identity matrix. This ensured that no state would become finite purely because of the perturbation, and threshold filters were used to ensure that all state values remained nonnegative. Perturbations were sampled independently across states and time steps.

2.4.2. Generating Synthetic Observations

[26] The truth system output vector ($\mathbf{y_t^{truth}} = \{\theta_{1:9}^{truth}, LAI^{truth}\}$) was used to generate synthetic observations, $\mathbf{z_t}$. At every observation time, a remote sensing measurement process was simulated by drawing from the Gaussian distribution

$$\mathbf{z_t} \sim \mathrm{N}[\mathbf{y_t}, R_t]; R_t = \begin{bmatrix} R_t^{\theta} & 0 \\ 0 & R_t^{LAI} \end{bmatrix}. \tag{6a}$$

R_t^{LAI} and R_t^{θ} represent the observation error covariance matrixes related to LAI and θ observations, respectively. Synthetic observations have no spatial scale.

[27] Frequency and error properties of synthetic observations were guided by uncertainty in existing remote sensing data. Observations of θ_1 are available from SMOS at most major agricultural areas every 3 days with a spatial resolution of 50 km and approximate retrieval accuracy of error $\sim \pm 0.04\ m^3\ m^{-3}$ [*Kerr et al.*, 2010]. An improvement in spatial resolution (to 9 km) is expected with the launch of SMAP in 2014 [*Entekhabi et al.*, 2010]. Measurement accuracy will degrade as vegetation water content, θ_{veg} (kg m^{-2}), increases throughout the growing season; in the

Table 5. Forcing Data Perturbation Sampling Parameters

				Correlations			
Weather Inputs	Multiplicative or Additive	Standard Deviation	AR(1) Coeffient[a]	Temperature	Radiation	Precipitation	Data Units[b]
Temperature (maximum and minimum)	A	1	1/e	1	−0.80	−0.32	°C
Solar Radiation	M	0.3	1/e	−0.80	1	0.40	MJ m^{-2} d
Precipitation	M	0.5	1/e	−0.32	0.40	1	mm

[a]First-order autoregressive coefficients assume a daily time series.
[b]Data units are the dimensions of the forcing data itself and not the units of the perturbations except in the case of temperature which uses additive perturbations; radiation and precipitation perturbations are multiplicative and unitless.

case of SMAP, observations at or better than the ± 0.04 $m^3\,m^{-3}$ accuracy level are expected to be confined to areas with vegetation water content less than 5 kg m^{-2} [*Entekhabi et al.*, 2010]. *Jackson and Schmugge* [1991] developed a relationship between vegetation water content and vegetation transmissivity, as proposed by *Kirdiashev et al.* [1979], which *Bolten et al.* [2010] adapted to model soil moisture observation uncertainty as

$$R_t^{\theta} = R_0 \exp\left(\frac{b\theta_{veg}}{2\cos(\phi)}\right). \tag{6b}$$

R_t^{θ} (m^6/m^6) is the variance of the soil moisture retrieval at time t made over vegetation, R_0 (m^6/m^6) is the variance of estimates made over bare soil, b is an environment parameter which accounts for vegetation type and roughness, and ϕ (degrees) is the satellite incidence angle. The SMAP incidence angle is 40° and we adopted the value of $b = 0.12$ for agricultural crops [*Crow et al.*, 2005], along with a bare soil observation error standard deviation of $(R_0)^{1/2} = 0.027$ $m^3\,m^{-3}$ resulting in a retrieval accuracy model which approaches $(R_t^{\theta})^{1/2} = 0.04$ $m^3\,m^{-3}$ as vegetation water content approaches $\theta_{veg} = 5$ kg m^{-2}. Vegetation water content was assumed to be a constant fraction of plant biomass and plant population (p_{pop} (plants/m^2)):

$$\theta_{veg} = \left(\frac{\alpha\beta p_{pop}}{1-\alpha}\right); \tag{6c}$$

$\alpha = 0.75$ was set according to results reported by *Malhotra* [1933]. Plant population is a CC component that is not included in the EnKF update.

[28] Synthetic observations of $\theta_{1:9}$ were generated every 3 days, each layer perturbed independently with the same statistical error characteristics. Remote sensing platforms are only able to measure soil water content in the upper few centimetres of soil, and in section 3.2 we compare assimilations which used only θ_1 observations with assimilations which used observations of $\theta_{1:9}$.

[29] The MODIS MOD15A2 product group provides LAI ($m^2\,m^{-2}$) estimates as an 8 day composite. The accuracy and uncertainty in this product has been investigated over agricultural areas by comparing the composite image to reference LAI from a single day at the end of the composite period; the uncertainty standard deviation was reported to be $(R_t^{LAI})^{1/2} \leq 0.38$ $m^2\,m^{-2}$ [*Tan et al.*, 2005]. We generated synthetic LAI observations with $(R_t^{LAI})^{1/2} = 0.38$ every 8 days to simulate the remote sensing measurement process.

2.4.3. Ensemble Size Experiments

[30] Ensemble size represents a balance between pdf representation and computation expense. Effects of varying ensemble size were evaluated using ensembles of $N_{ens} =$ 10, 25, 50, 75, 100, 250, 500, 750, and 1000. An appropriate ensemble size was found when pdf predictions of grain weight, LAI and θ_1 became stable with increasing sample size. The quality of ensemble representations of outputs LAI and θ_1 and state grain weight was quantified using the root mean square error (RMSE) taken over all simulation time steps of the difference between mean ensemble predicted output values and the true value.

[31] To make direct comparisons between OSSEs with different ensemble sizes, it was necessary to use the same truth system and observation set. Four truth systems were chosen and, for each truth system, a corresponding set of observations were generated and an $N_{ens} = 1,000$ member ensemble was sampled from the full uncertainty pdf outlined in Tables 4 and 5 and equation (5a). For each truth system, each ensemble of increasing size completely contained all smaller ensembles. For example, for a given truth system, the $N_{ens} = 25$ member ensemble contained the $N_{ens} = 10$ member ensemble plus 15 additional simulations. The RMSE averaged over these four experiments is reported, and the particular choice of ensemble size is discussed in section 3.1.

2.4.4. Modeling Uncertainty Experiments

[32] Once an appropriate ensemble size was chosen, experiments were conducted to test the ability of data assimilation to mitigate particular types of modeling uncertainty in yield estimates. Modleing uncertainty pdf were taken as marginal distributions of the entire joint uncertainty distribution (Tables 4 and 5 and equation (5a)). We tested the full joint uncertainty pdf described in section 2.4.1 plus five marginal uncertainty pdf related to (1) weather forcing data (Table 5), (2) soil parameters and initial conditions (Table 4), (3) cultivar parameters (Table 4), (4) model state perturbations (equation (5a)) to states listed in Table 3 except for grain weight, cumulative development units and cumulative germination units, and (5) same as point 4 but with perturbations to cumulative development units and cumulative germination units. Because each uncertainty type was independent from all others, marginalizing a particular uncertainty component was done by setting all of the variances of its uncertainty components to zero.

[33] Assimilation OSSEs were run for simulations of water-limited (Swift Current) and energy-limited (Rothamsted) crops using four types of observation sets: LAI and θ_1, LAI only, θ_1 only, and $\theta_{1:9}$; the first three represent what are available from satellites and the fourth provides a way to assess limitations of only having surface level soil moisture information. Each OSSE was repeated fifty times with different truth systems, ensembles and observations. The results were evaluated using a mean error score (ME (kg ha^{-1})), which is the absolute difference between the ensemble mean predicted end-of-season yield and the true yield. This was calculated for the open loop, EnKF, and SIRF ensembles for each of 50 OSSEs, and a single-tailed, two-sample t test ($\alpha = 0.05$) was used to test for a significant reduction in mean ME score due to SIRF or EnKF assimilation.

[34] Yield estimates can only be expected to improve when there are strong (although possibly indirect) relationships between model outputs and grain weight. Since grain weight is related to LAI and water stress through biomass, we report the absolute time-averaged Pearson product-moment correlation coefficients ($|\overline{\rho}|$) between model outputs and β. For $\theta_{1:9}$ the sum of profile water was used. Statistics were calculated using all open loop ensemble members from the 50 combined uncertainty OSSEs.

2.4.5. Observation Uncertainty Experiments

[35] Eight sets of OSSEs which utilized the full modeling uncertainty pdf were used to test effects of observation

uncertainty on assimilation results. Synthetic observations of LAI and θ_1 were generated and assimilated every 3 and 8 days as described in section 2.4.2; however, θ error variances were $(R^{\theta})^{(1/2)} = 0.001$, 0.005, 0.010, 0.015, 0.020, 0.030, 0.040, and 0.050 $(m^3\,m^{-3})$ and LAI error variances were $(R^{LAI})^{(1/2)} = 0.01$, 0.02, 0.05, 0.10, 0.15, 0.20, 0.30, and 0.40 for the eight sets of OSSEs. For both water-limited and energy-limited crops each observation type and uncertainty level was tested using fifty Monte Carlo OSSEs and the reduction in ME scores was used to evaluate EnKF and SIRF performance.

3. Results

3.1. Ensemble Size Experiments

[36] Figure 3 illustrates RMSE output and grain weight dynamics due to varying ensemble size averaged over four sets of Swift Current OSSEs. Generally, when LAI was assimilated LAI RMSE improved but not θ_1 RMSE, and when θ_1 was assimilated θ_1 RMSE improved but not LAI RMSE; this is similar to the findings of *Pauwels et al.* [2007], who used the EnKF and observed little improvement to modeled LAI when θ_1 observations were assimilated. In both cases where outputs improved (LAI RMSE for LAI assimilation and θ_1 RMSE for θ_1 assimilation) output RMSE values were relatively stable with increasing ensemble size after about $N_{ens} = 25$ for both the EnKF and SIRF. In the two cases where outputs did not improve (θ_1 RMSE for LAI assimilation and LAI RMSE for θ_1 assimilation) output RMSE values stabilized around $N_{ens} = 100$. *de Wit and van Diepen* [2007] used the EnKF and found stability in mean-square error of modeled LAI with EnKF assimilation of θ_1 at around $N_{ens} = 100$, which is in agreement with our findings. The grain weight state RMSE generally improved when LAI observations were assimilated but not θ_1 observations; in both cases, the grain weight RMSE became relatively stable around $N_{ens} = 100$. The remainder of the OSSEs discussed in this paper used an ensemble size of $N_{ens} = 100$.

3.2. Modeling Uncertainty Experiments

[37] Table 6 reports Monte Carlo average ME scores and time-averaged correlations between outputs and end-of-season yield for water-limited and energy-limited OSSEs. The results for each uncertainty type are described below. It is important to understand that the time-averaged correlations between model outputs and biomass inform assimilation results, but that the relationship is indirect and situation dependent. Thus the $|\overline{\rho}|$ coefficients in Table 6 cannot be compared directly.

3.2.1. Weather Inputs

[38] Precipitation uncertainty affects grain development indirectly via the water stress control on the leaf weight component of biomass, while radiation and temperature

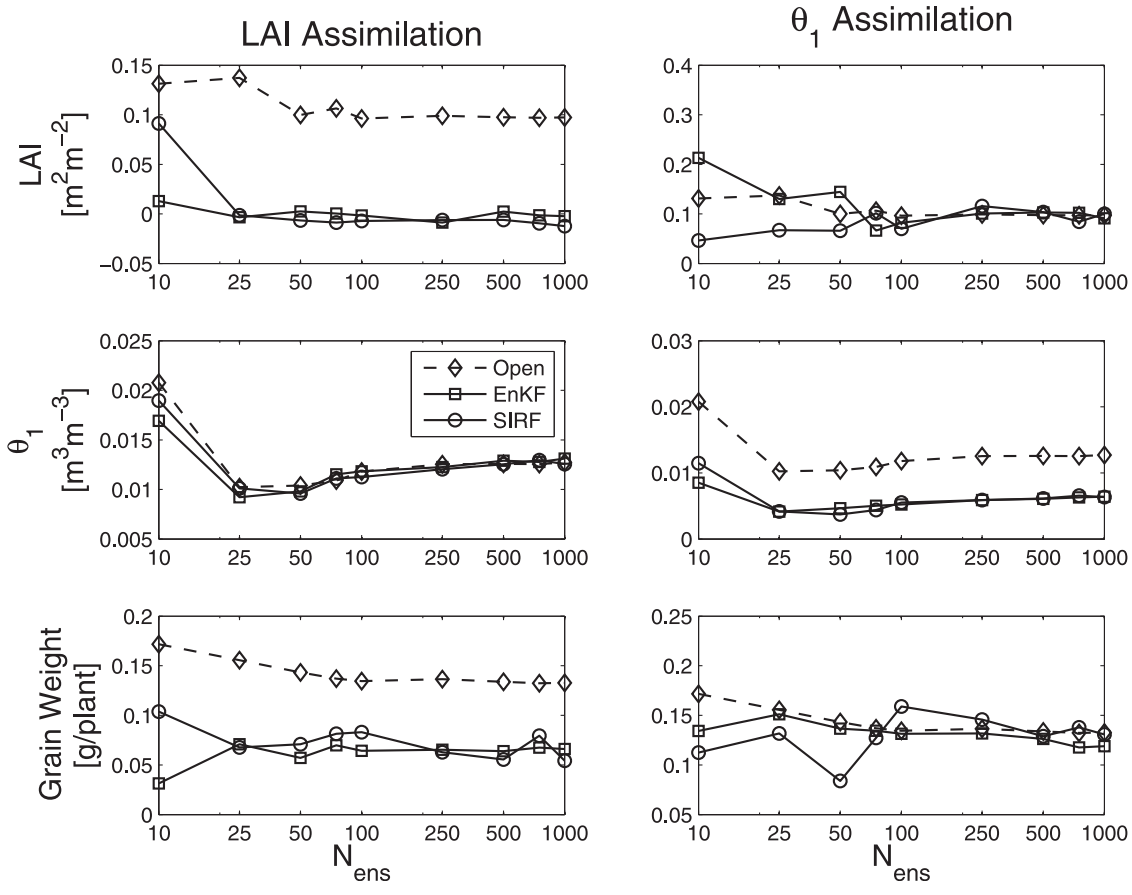

Figure 3. Output and grain weight time-averaged open loop, EnKF, and SIRF root-mean-square error values as a function of increasing ensemble size.

Table 6. Monte Carlo Average Mean Error Scores and Time-Averaged Correlation Coefficients for Modeling Uncertainty OSSEs[a]

Crop System	Uncertainty	Open Loop	EnKF				SIRF				$\lvert\overline{\rho}\rvert$		
			LAI and θ_1	LAI	θ_1	$\theta_{1:9}$	LAI and θ_1	LAI	θ_1	$\theta_{1:9}$	LAI	θ_1	$\theta_{1:9}$
Water limited (Swift Current)	Weather	243.7	280.2	255.2	280.0	299.3	219.1	219.1	213.7	**183.1**	0.548	0.490	0.572
	Soil parameters and initial conditions	322.6	287.3	311.9	297.9	616.4	427.0	377.3	620.7	**239.3**	0.918	0.088	0.233
	Cultivar parameters	375.5	366.2	364.3	373.9	386.0	414.9	375.9	396.7	394.6	0.964	0.286	0.461
	State perturbations without stage timing	604.8	**470.0**	**484.0**	555.3	**296.4**	**477.2**	**479.5**	544.4	**471.6**	0.845	0.115	0.780
	State perturbations with stage timing	587.4	543.9	556.5	589.4	500.9	547.1	533.1	637.6	653.1	0.657	0.120	0.159
	Combined sources	710.9	660.8	642.9	738.3	756.7	721.4	652.5	776.4	722.0	0.568	0.164	0.131
Energy limited (Rothamsted)	Weather	330.7	**275.2**	**274.4**	330.7	330.7	307.9	315.3	322.2	**244.5**	0.808	0.421	0.656
	Soil parameters and initial conditions	0.7	0.7	0.7	0.7	0.7	0.8	0.9	0.7	0.7	0.879	0.034	0.047
	Cultivar parameters	1352.5	1330.8	1320.7	1352.5	1352.5	1400.3	1319.2	1405.0	1359.9	0.770	0.607	0.054
	State perturbations without stage timing	356.8	382.3	356.7	360.5	364.4	406.3	367.2	366.0	545.2	0.341	0.007	0.005
	State perturbations with stage timing	1034.9	1084.9	1081.6	999.5	1024.6	1005.2	**722.9**	1040.8	1383.5	0.452	0.038	0.004
	Combined sources	1342.3	1227.8	1180.2	1330.8	1303.6	1172.2	1217.5	1405.0	1870.0	0.645	0.101	0.234

[a]Bold values indicate a significant reduction in mean error score by assimilation ($\alpha = 0.05$). OSSE, observing system simulation experiment; SIRF, sequential importance resampling filter; LAI, leaf area index.

affect grain development directly as well as indirectly though biomass. In simulations of the water-limited crop, LAI and θ were correlated with β at approximately $|\overline{\rho}| = 0.5$. ME scores were not significantly improved by assimilating LAI or θ_1 using either filter. The inefficiency in assimilating LAI observations can be attributed to differences in the way radiation and temperature affect leaf and grain development and the fact that uncertainty in radiation and temperature affected grain growth after leaves were senesced (Figure 2).

[39] The SIRF was able to reduce the average ME score by assimilating $\theta_{1:9}$ and was more successful than the EnKF, in this case likely because of the EnKF's linear model assumption. Swapping out state vectors for ones from ensemble members which represent crops grown in conditions similar to the truth system (similar historical water demand and availability) improved yield predictions; however, updating plant states on the basis of linear correlations with soil states was inefficient, and improvements to estimates of profile water content did not translate into improved simulations of future plant development. The useful information stored in the soil moisture state was information about growth histories; this suggests that an improved understanding of the effects of weather on the crop growth environment might not be as important as an improved understanding of the effects of weather on crops themselves.

[40] In energy-limited simulations, LAI was correlated with β at $|\overline{\rho}| = 0.8$ and EnKF assimilation of LAI observations improved yield predictions. Water stress was a decorrelating factor between LAI and biomass because of differences in how leaf weight, stem weight, and reserves weight responded to stress. Again, in the energy-limited environment, SIRF assimilation of $\theta_{1:9}$ improved yield estimates while the EnKF did not.

3.2.2. Soil Parameters and Initial Conditions

[41] In simulations of the water-limited crop, the ability of the soil to infiltrate and store water was important for productivity. Correlations between LAI and β were high ($|\overline{\rho}| = 0.918$); however, assimilation of LAI did not result in improved yield estimates. In this case, when the filters increased biomass because of high LAI observations, large plants were essentially placed into soils that could support them. When the filters decreased biomass because of low LAI observations, the plants grew quickly because of sufficient water availability. This is an example of the limitations of data assimilation filters when model parameters are uncertain. Since LAI observations were not available after senescence (Figure 2), the updated plant simulations were able to respond to the new environment before grain growth was completed.

[42] In contrast, correlation between $\theta_{1:9}$ and β was moderate ($|\overline{\rho}| = 0.233$); however, the SIRF was able to improve ME scores by assimilating $\theta_{1:9}$. In this case, since observations of soil moisture were available through the end of the growing season, the SIRF was able to replace the ensemble of plant state vectors late in the grain development phase with ensemble members which had developed in conditions similar to the truth system.

[43] Surface level soil moisture observations contained insufficient information to improve grain weight simulations

because surface soil layer parameters were independent of root zone parameters and the root zone largely controls water availability. In the low-stress simulations, soil parameters did not affect grain growth.

3.2.3. Cultivar Parameters

[44] Error in yield estimates due to uncertainty in cultivar parameters was not mitigated by state updating for either crop using any combination of filter and observations. Correlations between LAI and β were high, but differences in the kernel number and standard kernel size parameters decoupled β from grain weight. LAI and θ observations do not inform these parameter values.

3.2.4. State Perturbations Without Stage Timing States

[45] When states other than stage timing variables cumulative development units and cumulative germination units were perturbed, water-limited LAI was correlated with β ($|\overline{\rho}| = 0.845$), however in the energy-limited environment, it was not ($|\overline{\rho}| = 0.341$). In the water-limited environment, perturbations to the root zone soil water state partially controlled growth variations through the stress factor, and this resulted in correlated LAI and β. In the energy-limited case, LAI and β were not well correlated because the state perturbations were independent. Thus in the water-limited environment, LAI assimilation resulted in improved ME score, and in the energy-limited environment, it did not.

[46] Note that θ_1 was not well correlated with β in either set of simulations; however, $\theta_{1:9}$ was correlated in the water-limited environment. Again, this is because perturbations to soil water states were independent between layers and root zone water availability determined water stress. $\theta_{1:9}$ assimilation improved yield estimates in this case.

3.2.5. State Perturbations Including Stage Timing States

[47] When perturbations to stage timing states cumulative development units and cumulative germination units were included, the water-limited LAI-β correlation was reduced ($|\overline{\rho}| = 0.845$ to $|\overline{\rho}| = 0.657$). Differences in growth stages between ensemble simulations accumulated throughout the growing season and caused a gradual decrease in cross correlation between vegetation states (not shown). In energy-limited simulations, the correlation increased slightly ($|\overline{\rho}| = 0.341$ to $|\overline{\rho}| = 0.452$) and the SIRF was able to improve ME scores by assimilating LAI. In the water-limited case, stress controlled biomass and LAI through leaf development and dissimilar development stage transitions resulted in decorrelation. In the energy-limited case, random perturbations controlled leaf development, stem weight, and reserves weight independently and similar development stage transitions resulted in slightly higher correlated vegetation states.

3.2.6. Combined Uncertainty Sources

[48] In a full modeling uncertainty paradigm, the EnKF and SIRF were unable to significantly improve ME scores in any case. This is a combined result of lack in state correlations caused by differences in cultivar parameters and differences in weather controls on biomass, LAI and grain weight.

3.3. Observation Uncertainty Experiments

[49] Results from varying error variances of synthetic LAI and θ_1 observations (Table 7) suggest that even nearly perfect observations of surface level soil moisture will not improve single season yield estimates under reasonable modeling uncertainty assumptions. LAI assimilation was valuable in the water-limited simulations when the LAI observations error standard deviation was between 0.05 and 0.30 [$m^2\ m^{-2}$]. The SIRF was almost always better at assimilating LAI in the water-limited simulations, which is likely due to the highly nonlinear nature of the CC module.

4. Discussion

[50] The purpose of this study was to identify potential for state-updating data assimilation to mitigate error in yield estimates due to modeling uncertainty. Results show that

Table 7. Monte Carlo Average Mean Error Scores for Combined Modeling Uncertainty Assimilations With Increasing Observation Error Variance (Observation Error)[a]

		LAI			θ_1		
			Mean Error			Mean Error	
Crop System	Open Loop Mean Error	Observation Uncertainty	EnKF	SIRF	Observation Uncertainty	EnKF	SIRF
Water limited (Swift Current)	718.7	0.01	607.6	656.9	0.001	758.9	1054.6
	731.9	0.02	666.8	682.6	0.005	786.9	949.1
	701.5	0.05	609.8	**543.8**	0.010	750.5	760.6
	665.0	0.10	597.6	586.0	0.015	671.2	664.9
	705.8	0.15	**565.5**	**494.5**	0.020	681.7	771.1
	681.1	0.20	**551.7**	**524.2**	0.030	707.7	745.1
	752.4	0.30	631.2	**609.0**	0.040	732.9	760.4
	666.7	0.40	559.5	572.2	0.050	670.1	658.9
Energy limited (Rothamsted)	1314.1	0.01	1394.0	1528.6	0.001	1300.3	2111.5
	1296.0	0.02	1321.9	1232.0	0.005	1304.0	1922.3
	1360.6	0.05	1377.2	1341.2	0.010	1351.9	1865.5
	1572.4	0.10	1626.2	1435.2	0.015	1594.3	1776.3
	1744.9	0.15	1785.2	**1278.0**	0.020	1727.6	2074.9
	1383.5	0.20	1397.3	1342.1	0.030	1413.2	1513.7
	1454.7	0.30	1345.2	1352.5	0.040	1438.6	1353.1
	1472.9	0.40	1460.0	1330.3	0.050	1419.9	1731.0

[a]Bold values indicate a significant reduction in mean error score by assimilation ($\alpha = 0.05$).

this approach was generally unable to improve yield estimates under realistic uncertainty scenarios. There were many factors which contribute to this: (1) weather inputs affect grain and leaf growth differently meaning that similar LAI outputs do not imply similar grain weight states, (2) that certain cultivar parameters affect grain development directly in a way which is independent of all other model states, (3) that state updating often results in plant state vectors which disagree with model (soil) parameters, and (4) that surface level soil moisture observations did not contain sufficient information about available water and water stress. Results suggest that in water-limited environments, LAI assimilation would be more useful if observation error was lower than what is currently available. This is a problem because LAI observations will suffer from uncertainties which were not considered in this study, namely, spatial heterogeneity in agricultural systems and discrepancies in spatial resolutions between fields and image pixels.

[51] These findings are qualitatively similar to those from the case study reported by *de Wit and van Diepen* [2007], who used the EnKF to assimilate θ_1 observations over crop land in Europe. They found improvement to winter wheat yield estimates in 33 out of 88 test regions. Although their real-world experiment was likely hampered by mismatches in spatial resolution between agricultural fields and remote sensing observations, as well as other spatial factors including crop heterogeneity, we have shown that these factors alone were likely not the reason for poor assimilation results.

[52] This study suggests that in order to combine remote sensing observations with agricultural models for the purpose of estimating yield at single-season time scales, it will be necessary to modify our interpretation of crop development. Primarily, it would be interesting to investigate methods and ancillary data necessary for correlating leaf development with grain development directly. It is likely that the utility of soil moisture observations will be limited to monitoring extreme events over large time scales as was implied by *Bolten et al.* [2010], or for estimating irrigation schedules and agricultural water use as was done by *Wang and Cai* [2007].

[53] **Achnowledgements.** This research was jointly supported by a grant from the NASA Terrestrial Ecology program entitled "Ecological and agricultural productivity forecasting using root-zone soil moisture products derived from the NASA SMAP mission" (principal investigator W. T. Crow), the NASA SMAP Science Definition Team, and grant 08-SMAPSDT08-0042 (principal investigator M. S. Moran). The authors would like to thank Cheryl Porter from the Department of Agricultural and Biological Engineering at the University of Florida for her help acquiring and managing DSSAT source code.

References

Arnold, C. P., and C. H. Dey (1986), Observing-systems simulation experiments: Past, present, and future, *Bull. Am. Meteorol. Soc.*, *67*(6), 687–695, doi:10.1175/1520-0477(1986)067<0687:OSSEPP>2.0.CO;2.

Bolten, J. D., W. T. Crow, X. W. Zhan, T. J. Jackson, and C. A. Reynolds (2010), Evaluating the utility of remotely sensed soil moisture retrievals for operational agricultural drought monitoring, *IEEE J. Sel. Top. Appl. Earth Obs. Remote Sens.*, *3*(1), 57–66, doi:10.1109/JSTARS.2009.2037163.

Campbell, C. A., D. R. Cameron, W. Nicholaichuk, and H. R. Davidson (1977a), Effects of fertilizer N and soil moisture on growth, N content, and moisture use by spring wheat, *Can. J. Soil Sci.*, *57*(3), 289–310, doi:10.4141/cjss77-036.

Campbell, C. A., H. R. Davidson, and F. G. Warder (1977b), Effects of fertilizer N and soil moisture on yield, yield components, protein content and N accumulation in aboveground pars of spring wheat, *Can. J. Soil Sci.*, *57*(3), 311–327, doi:10.4141/cjss77-035.

Cosby, B. J., G. M. Hornberger, R. B. Clapp, and T. R. Ginn (1984), A statistical exploration of the relationships of soil moisture characteristics to the physical properties of soils, *Water Resour. Res.*, *20*(6), 682–690, doi:10.1029/WR020i006p00682.

Crow, W. T., R. D. Koster, R. H. Reichle, and H. O. Sharif (2005), Relevance of time-varying and time-invariant retrieval error sources on the utility of spaceborne soil moisture products, *Geophys. Res. Lett.*, *32*, L24405, doi:10.1029/2005GL024889.

de Wit, A. M., and C. A. van Diepen (2007), Crop model data assimilation with the ensemble Kalman filter for improving regional crop yield forecasts, *Agric. For. Meteorol.*, *146*(1–2), 38–56, doi:10.1016/j.agrformet.2007.05.004.

Entekhabi, D., et al. (2010), The soil moisture active passive (SMAP) mission, *Proc. IEEE*, *98*(5), 704–716, doi:10.1007/s10236-003-0036-9.

Evensen, G. (2003), The ensemble Kalman filter: Theoretical formulation and practical implementation, *Ocean Dyn.*, *53*, 343–367, doi:10.1007/s10236-003-0036-9.

Gordon, N. J., D. J. Salmond, and A. F. M. Smith (1993), Novel approach to nonlinear non-Gaussian Bayesian state estimation, *IEE Proc., Part F, Radar Signal Process.*, *140*(2), 107–113, doi:10.1049/ip-f-2.1993.0015.

Hoogenboom, G., et al. (2004), Decision support system for agrotechnology transfer version 4.0, technical report, Univ. of Hawaii, Honolulu.

Houtekamer, P. L., and H. L. Mitchell (2001), A sequential ensemble Kalman filter for atmospheric data assimilation, *Mon. Weather Rev.*, *129*(1), 123–137, doi:10.1175/1520-0493(2001)129<0123:ASEKFF>2.0.CO;2.

Jackson, T. J., and T. J. Schmugge (1991), Vegetation effects on the microwave emission of soils, *Remote Sens. Environ.*, *36*(3), 203–212, doi:10.1016/0034-4257(91)90057-D.

Jones, J. W., G. Hoogenboom, C. H. Porter, K. J. Boote, W. D. Batchelor, L. A. Hunt, P. W. Wilkens, U. Singh, A. J. Gijsman, and J. T. Ritchie (2003), The DSSAT cropping system model, *Eur. J. Agron.*, *18*(3–4), 235–265, doi:10.1016/S1161-0301(02)00107-7.

Kerr, Y. H., et al. (2010), The SMOS mission: New tool for monitoring key elements of the global water cycle, *Proc. IEEE*, *98*(5), 666–687, doi:10.1109/jproc.2010.2043032.

Kirdiashev, K., A. Chukhlantsev, and A. Shutko (1979), Microwave radiation of the Earth's surface in the presence of vegetation cover, *Radiotekh. Elektron. (Moscow, Russ. Fed.)*, *24*, 256–264.

Knyazikhin, Y., et al. (1999), *MODIS Leaf Area Index (LAI) and Fraction of Photosynthetically Active Radiation Absorbed by Vegetation (FPAR) Product (MOD15) Algorithm Theoretical Basis Document*, NASA Goddard Space Flight Center, Greenbelt, MD.

Liu, Y. Q., and H. V. Gupta (2007), Uncertainty in hydrologic modeling: Toward an integrated data assimilation framework, *Water Resour. Res.*, *43*, W07401, doi:10.1029/2006WR005756.

Malhotra, R. (1933), A contribution to the biochemistry of the wheat plant, *J. Biochem.*, *18*(2), 199–205.

McLaughlin, D. (2002), An integrated approach to hydrologic data assimilation: Interpolation, smoothing, and filtering, *Adv. Water Resour.*, *25*(8–12), 1275–1286, doi:10.1016/S0309-1708(02)00055-6.

Mo, X. G., S. X. Liu, Z. H. Lin, Y. Q. Xu, Y. Xiang, and T. R. McVicar (2005), Prediction of crop yield, water consumption and water use efficiency with a SVAT-crop growth model using remotely sensed data on the North China Plain, *Ecol. Modell.*, *183*(2–3), 301–322, doi:10.1016/j.ecolmodel.2004.07.032.

Moulin, S., A. Bondeau, and R. Delecolle (1998), Combining agricultural crop models and satellite observations: From field to regional scales, *Int. J. Remote Sens.*, *19*(6), 1021–1036, doi:10.1080/014311698215586.

Njoku, E., T. Jackson, V. Lakshmi, T. Chan, and S. Nghiem (2003), Soil moisture retrieval from AMSR-E, *IEEE Trans. Geosci. Remote Sens.*, *41*, 215–229, doi:10.1109/TGRS.2002.808243.

Pauwels, V. R. N., N. E. C. Verhoest, G. J. M. De Lannoy, V. Guissard, C. Lucau, and P. Defourny (2007), Optimization of a coupled hydrology-crop growth model through the assimilation of observed soil moisture and leaf area index values using an ensemble Kalman filter, *Water Resour. Res.*, *43*, W04421, doi:10.1029/2006WR004942.

Pellenq, J., and G. Boulet (2004), A methodology to test the pertinence of remote-sensing data assimilation into vegetation models for water and energy exchange at the land surface, *Agronomie*, *24*, 197–204, doi:10.1051/agro:2004017.

Prévot, L., H. Chauki, D. Troufleau, M. Weiss, F. Baret, and N. Brisson (2003), Assimilating optical and radar data into the stics crop model for wheat, *Agronomie*, *23*(4), 297–303, doi:10.1051/agro:2003003.

Priestley, C., and R. J. Taylor (1972), Assessment of surface heat flux and evaporation using large-scale parameters, *Mon. Weather Rev.*, *100*(2), 81–92, doi:10.1175/1520-0493(1972)100< 0081:OTAOSH>2.3.CO;2.

Reichle, R. H. (2008), Data assimilation methods in the Earth sciences, *Adv. Water Resour.*, *31*(11), 1411–1418, doi:10.1016/j.advwatres.2008.01.001.

Reichle, R. H., R. D. Koster, P. Liu, S. P. P. Mahanama, E. G. Njoku, and M. Owe (2007), Comparison and assimilation of global soil moisture retrievals from the Advanced Microwave Scanning Radiometer for the Earth Observing System (AMSR-E) and the Scanning Multichannel Microwave Radiometer (SMMR), *J. Geophys. Res.*, *112*, D09108, doi:10.1029/2006JD008033.

Reichle, R. H., S. V. Kumar, S. P. P. Mahanama, R. D. Koster, and Q. Liu (2010), Assimilation of satellite-derived skin temperature observations into land surface models, *J. Hydrometeorol.*, *11*(5), 1103–1122, doi:10.1175/2010JHM1262.1.

Richie, J. (1998), *Soil Water Balance and Plant Water Stress*, pp. 41–54, Kluwer Acad., Dordrecht, Netherlands.

Tan, B., J. N. Hu, P. Zhang, D. Huang, N. Shabanov, M. Weiss, Y. Knyazikhin, and R. B. Myneni (2005), Validation of Moderate Resolution Imaging Spectroradiometer leaf area index product in croplands of Alpilles, France, *J. Geophys. Res.*, *110*, D01107, doi:10.1029/2004JD004860.

Wang, D. B., and X. M. Cai (2007), Optimal estimation of irrigation schedule: An example of quantifying human interferences to hydrologic processes, *Adv. Water Resour.*, *30*(8), 1844–1857, doi:10.1016/j.advwatres.2007.02.006.

W. T. Crow, Hydrology and Remote Sensing Laboratory, ARS, USDA, 10300 Baltimore Ave., Bldg. 007, Rm. 104, BARC-West, Beltsville, MD 20705, USA. (wade.crow@ars.usda.gov)

H. V. Gupta and G. S. Nearing, Department of Hydrology and Water Resources, University of Arizona, Harshbarger Bldg., Tucson, AZ 85721, USA. (hoshin.gupta@hwr.arizona.edu; grey@email.arizona.edu)

M. S. Moran, Southwest Watershed Research Center, ARS, USDA, 2000 E. Allen Rd., Tucson, AZ 85719, USA. (susan.moran@ars.usda.gov)

R. H. Reichle, NASA Goddard Space Flight Center, Bldg. 33, Rm. G-106, Greenbelt Rd., Greenbelt, MD 20771, USA. (rolf.reichle@nasa.gov)

K. R. Thorp, Arid-Land Agricultural Research Center, ARS, USDA, 21881 North Cardon Ln., Maricopa, AZ 85138, USA. (kelly.thorp@ars.usda.gov)